Growth of the Tian Shan Drives Migration of the Conglomerate-Sandstone Transition in the Southern Junggar Foreland Basin

Chao Li, Shengli Wang, Yongxiang Li, Yan Chen, Hugh Sinclair, Dongtao Wei, Delong Ma, Huayu Lu, Xianyan Wang, Liangshu Wang

AGU ADVANCING EARTH AND SPACE SCIENCE

Geophysical Research Letters®

RESEARCH LETTER
10.1029/2021GL097545

Key Points:

- We provide the first documentation of the migration of the conglomerate-sandstone transition (CST) preserved in foreland basin successions
- The CST in the southern Junggar foreland basin migrates northward at 0.4 ± 0.1 mm/yr along 84°E and at 4.0 ± 1.2 mm/yr along 87°E
- Deviations between the measured and predicted CST positions are modulated by climate change

Supporting Information:

Supporting Information may be found in the online version of this article.

Correspondence to:

S. Wang,
wangsl@nju.edu.cn

Citation:

Li, C., Wang, S., Li, Y., Chen, Y., Sinclair, H., Wei, D., et al. (2022). Growth of the Tian Shan drives migration of the conglomerate-sandstone transition in the southern Junggar foreland basin. *Geophysical Research Letters*, *49*, e2021GL097545. https://doi.org/10.1029/2021GL097545

Received 17 DEC 2021
Accepted 22 JAN 2022

Author Contributions:

Conceptualization: Shengli Wang, Yongxiang Li
Formal analysis: Chao Li
Funding acquisition: Chao Li, Shengli Wang
Investigation: Yan Chen
Methodology: Chao Li, Shengli Wang, Yongxiang Li, Yan Chen, Liangshu Wang
Resources: Dongtao Wei, Delong Ma, Liangshu Wang
Writing – original draft: Chao Li, Shengli Wang
Writing – review & editing: Chao Li, Shengli Wang, Yongxiang Li, Yan Chen, Hugh Sinclair, Huayu Lu, Xianyan Wang

Growth of the Tian Shan Drives Migration of the Conglomerate-Sandstone Transition in the Southern Junggar Foreland Basin

Chao Li[1,2], Shengli Wang[1], Yongxiang Li[1], Yan Chen[3], Hugh Sinclair[4], Dongtao Wei[5], Delong Ma[6], Huayu Lu[7], Xianyan Wang[7], and Liangshu Wang[1]

[1]Institute of Continental Geodynamics, School of Earth Sciences and Engineering, Nanjing University, Nanjing, China, [2]School of Earth Sciences and Engineering, Hohai University, Nanjing, China, [3]University Orléans, CNRS, BRGM, ISTO, UMR 7327, Orléans, France, [4]School of GeoSciences, University of Edinburgh, Edinburgh, UK, [5]Xi'an Center of China Geological Survey, Xi'an, China, [6]Research Institute of Petroleum Exploration and Development—Northwest, PetroChina, Lanzhou, China, [7]School of Geography and Ocean Science, Nanjing University, Nanjing, China

Abstract The conglomerate-sandstone transition (CST) preserved in foreland basins records the stratigraphic equivalent of the gravel to sand transition (GST) which migrates in response to shortening in steady state orogen-foreland basin systems. Two seismic profiles in the southern Junggar foreland basin provide the first seismic record of migrating CSTs and an opportunity to quantify its migration history in response to the growth of the northern Tian Shan. We identify the horizontal positions of the CSTs based on the distinct seismic signature of conglomerate versus sandstone and estimate their ages according to magnetostratigraphic sections. The linear-regression analysis reveals that the CSTs migrated northward at 0.4 ± 0.1 mm/yr along 84°E from ~23 to ~6 Ma and at 4.0 ± 1.2 mm/yr along 87°E from ~3.1 to ~0.7 Ma. The discrepancy relates to variations in crustal shortening along strike of the range. Temporal deviations in the CST positions suggest the second-order impacts of climatic change.

Plain Language Summary Rivers in foreland basins commonly exhibit a sharp gravel to sand transition of bed sediment (GST), which is preserved in the stratigraphy as the conglomerate-sandstone transition (CST). Previous studies attribute the migration of the CST in foreland basins to tectonics of the coupled mountain ranges. Migration of the CSTs is considered as a possible archive of long-term crustal shortening in an orogen-foreland basin system. In this study, we identify the horizontal position of the CST in the southern Junggar foreland basin north of the Tian Shan based on two seismic profiles. Ages of sedimentary layers imaged by the seismic profiles are estimated according to previous magnetostratigraphic investigations. A linear-regression analysis between positions and ages of the CSTs indicates the northward migration rates of the CSTs. The rates approximate the long-term crustal shortening rates in the northern Tian Shan orogen-foreland basin system. A discrepancy between the migration rates of the CSTs in the eastern and western segments reveals variations in crustal shortening along the range. This work demonstrates that migration of CSTs in a foreland basin setting can act as a proxy of crustal shortening in orogen-foreland basin systems.

1. Introduction

In an orogenic belt-foreland basin setting, sediments from the mountain are transported downstream and accumulate in foreland basins. Sediments routing through the network of rivers display downstream grain size fining due to sorting and abrasion (Paola et al., 1992). A grain size transition from gravel to sand, termed the gravel-sand transition (GST; Ferguson et al., 1996), occurs in a short downstream distance from the sediment source. The GST is preserved in the stratigraphy of a sedimentary basin as the conglomerate-sandstone transition (CST; e.g., Dubille & Lavé, 2015). The position of the CST in a foreland basin succession is determined by basin subsidence, sediment supply, and grain size (Allen et al., 2013; Armitage et al., 2011), and all these factors depend on the interactions of tectonics in the adjacent mountains and regional climate (Dingle et al., 2016, 2017; Duller et al., 2010; Quick et al., 2020). The propagation of the orogenic wedge toward to the foreland drives the forelandward migration of the coupled foreland basin system as well as sedimentary facies (Flemings & Jordan, 1989;

DeCelles & DeCelles, 2001; Dubille & Lavé, 2015; Sinclair et al., 1991). Hence, the migration of the CST in a foreland basin is primarily a result of crustal shortening between the orogenic wedge and the foreland basin, modulated by climate and lithology (e.g., Burbank et al., 1988; Dingle et al., 2016, 2017; Schlunegger & Norton, 2015). Previous studies attribute the progressive forelandward migration of the CST to orogenic tectonism, such as in the Ganga foreland basin (Dubille & Lavé, 2015; Quick et al., 2020) and the foreland basins on both sides of the Tian Shan (Charreau, Gumiaux, et al., 2009). Therefore, the evolution of the CST provides a potential proxy for long-term crustal shortening in an orogen-foreland basin system. This new proxy could complete the conventional means in quantitatively constraining the crustal shortening in orogen-foreland basin systems such as by studying active folding and faulting, constructing balanced cross sections, modeling growth of the contractional folds, and satellite geodetic surveys.

In this study, we provide the first documentation of the long-term (~20 Myr) migration of the CST in a foreland basin setting and relate it to along-strike variations in crustal shortening. The data are from the southern Junggar foreland basin (Figure 1), north of the Tian Shan mountain range where high-quality seismic profiles and well log data have been acquired for hydrocarbon exploration over the past two decades. Dating of the Cenozoic successions is constrained by magnetostratigraphic investigations (e.g., Charreau et al., 2005; Charreau, Chen, et al., 2009; Lu et al., 2010). By reconstructing the position of the CST through time, we demonstrate how its migration responds to the propagation of the northern Tian Shan orogenic wedge relative to the Junggar block, and how this varies along the strike of the range.

2. Geological Setting

The Tian Shan in Central Asia is one of the largest active intracontinental orogenic belts in the world (e.g., Cawood et al., 2009). This east-west trending range originated from accretion of several island arcs and collision of several continental blocks in the Paleozoic (Charvet et al., 2011; Windley et al., 1990). In the Mesozoic, the Tian Shan was reactivated, probably in response to the accretion in the southern margin of the Eurasian plate, especially in the Tibetan area (Bullen et al., 2001), as attested by thermochronological studies (e.g., Dumitru et al., 2001; Jolivet et al., 2010; Jepson et al., 2018, 2021; Macaulay et al., 2013; Sobel et al., 2006) and sedimentary deposits in the foreland area (e.g., Hendrix et al., 1992). The present-day topography of the Tian Shan has been interpreted to be the result of late Cenozoic deformation caused by the India-Asia collision (Avouac et al., 1993; Dumitru et al., 2001; Li et al., 2019, 2020; Molnar & Tapponnier, 1975). Topographic growth of the range induced flexural subsidence in the foreland basins on both sides of the Tianshan. On its northern side, the southern Junggar foreland basin contains an ~5,000 m thick Cenozoic succession that is divided into the Ziniquanzi, Anjihaihe, Shawan, Taxihe, Dushanzi, and Xiyu Formations (Fms) in an ascending order (BGMRX, 1993). The Anjihaihe, Shawan, Taxihe, and Dushanzi Fms thin and onlap northward and constitute the main units of the foreland basin (Wang et al., 2013, Figure 1c). Sedimentary facies suggest that depositional environments in the basin changed from lacustrine in the Oligocene to fluvial-alluvial fan environment since late Miocene times (Figure S2 in Supporting Information S1; BGMRX, 1993; Charreau, Gumiaux, et al., 2009).

3. Quantifying the Conglomerate-Sandstone Transition Migration

We study two near-north-south trending seismic reflection profiles across the foredeep of the southern Junggar foreland basin (Figure 1 and Figures S1, S5 in Supporting Information S1). Profile AA′, 23-km-long and 4-s-deep (Figure 2a), is located in the western part of the basin. Profile BB′, 30-km-long and 4-s-deep (Figure 2b), is located in the eastern part of the basin. Every reflector of these two profiles above the base of the Anjihaihe Fm displays two distinct styles of seismic phases: high amplitude, semicontinuous, and hummocky to the south and high amplitude and continuous to the north (Figures 2a and 2b). Based on well log data and our field observations on the position of the gravel-sand transition in the modern rivers (Figure 1b), we interpret that the southern semicontinuous and hummocky phase represents amalgamated gravelly channel deposits, and the northern continuous phase represents sandstone-dominated channel and floodplain deposits (e.g., He et al., 2005; Charreau, Gumiaux, et al., 2009). Therefore, the contrast in the style of seismic phases is interpreted as an indicator of lithology change marking the CST of a sedimentary layer.

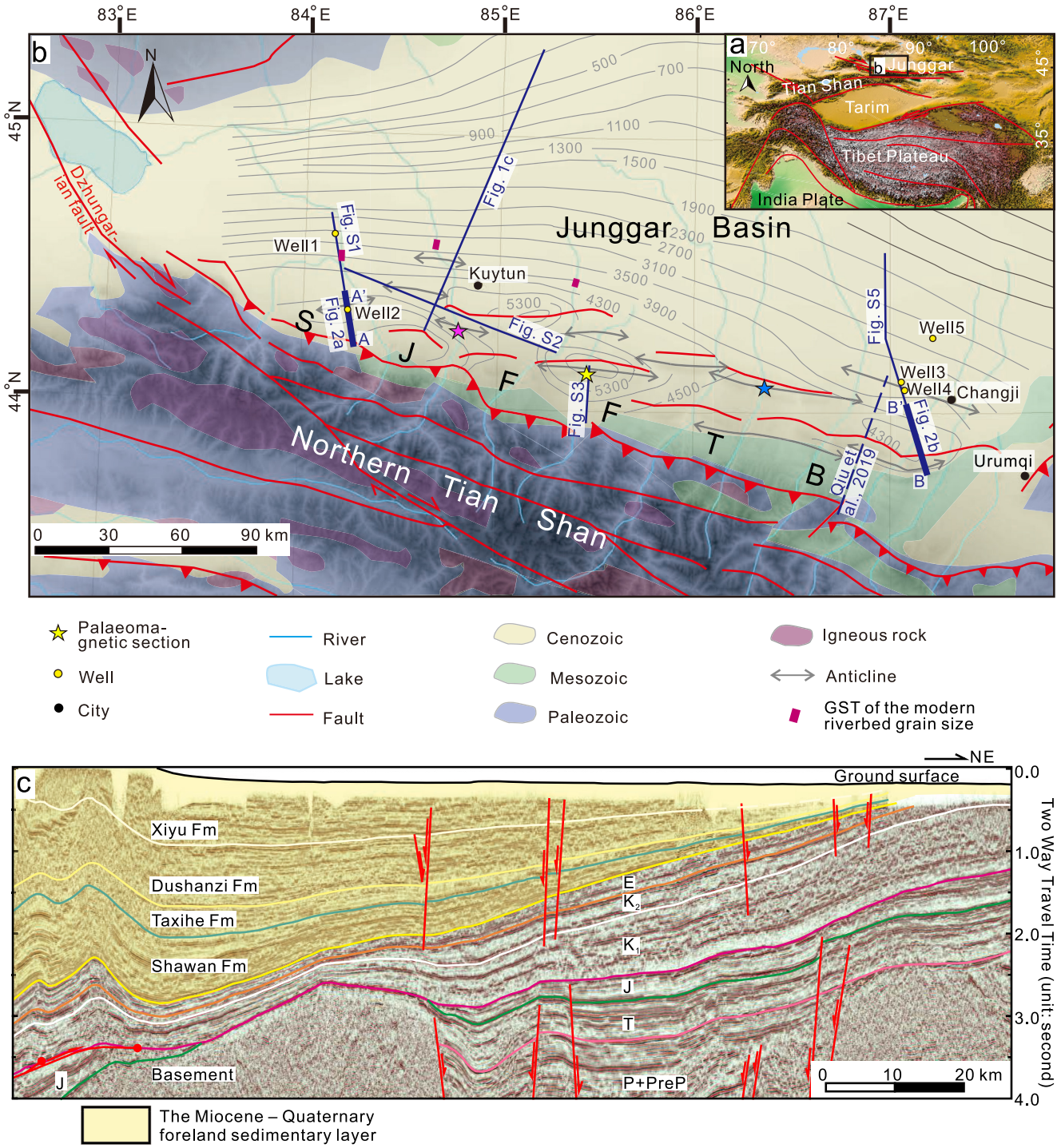

Figure 1. (a) Location of the northern Tian Shan mountain range within the India-Asia collision system. (b) Thickness contours (unit: m) of the Neogene successions in the southern Junggar foreland basin (Lv, 2005). Locations of profile AA′ and BB′ (Figures 2a and 2b) are marked by the thick dark blue lines and locations of Figure 1c and Figures S1, S2, S3, and S5 in Supporting Information S1 are marked by the thin dark blue lines. The purple, yellow, and blue stars mark the magnetostratigraphic sections from Charreau et al. (2005); Charreau, Chen, et al. (2009) and Lu et al. (2010), respectively. Southern Junggar foreland fold-thrust belt (SJFFTB) is an abbreviation for the southern Junggar foreland fold-thrust belt. (c) A seismic profile across the southern Junggar foreland basin (modified from Wang et al., 2013) shows that the Shawan, Taxihe, Dushanzi, and Xiyu Formations form a typical foreland sedimentary prism.

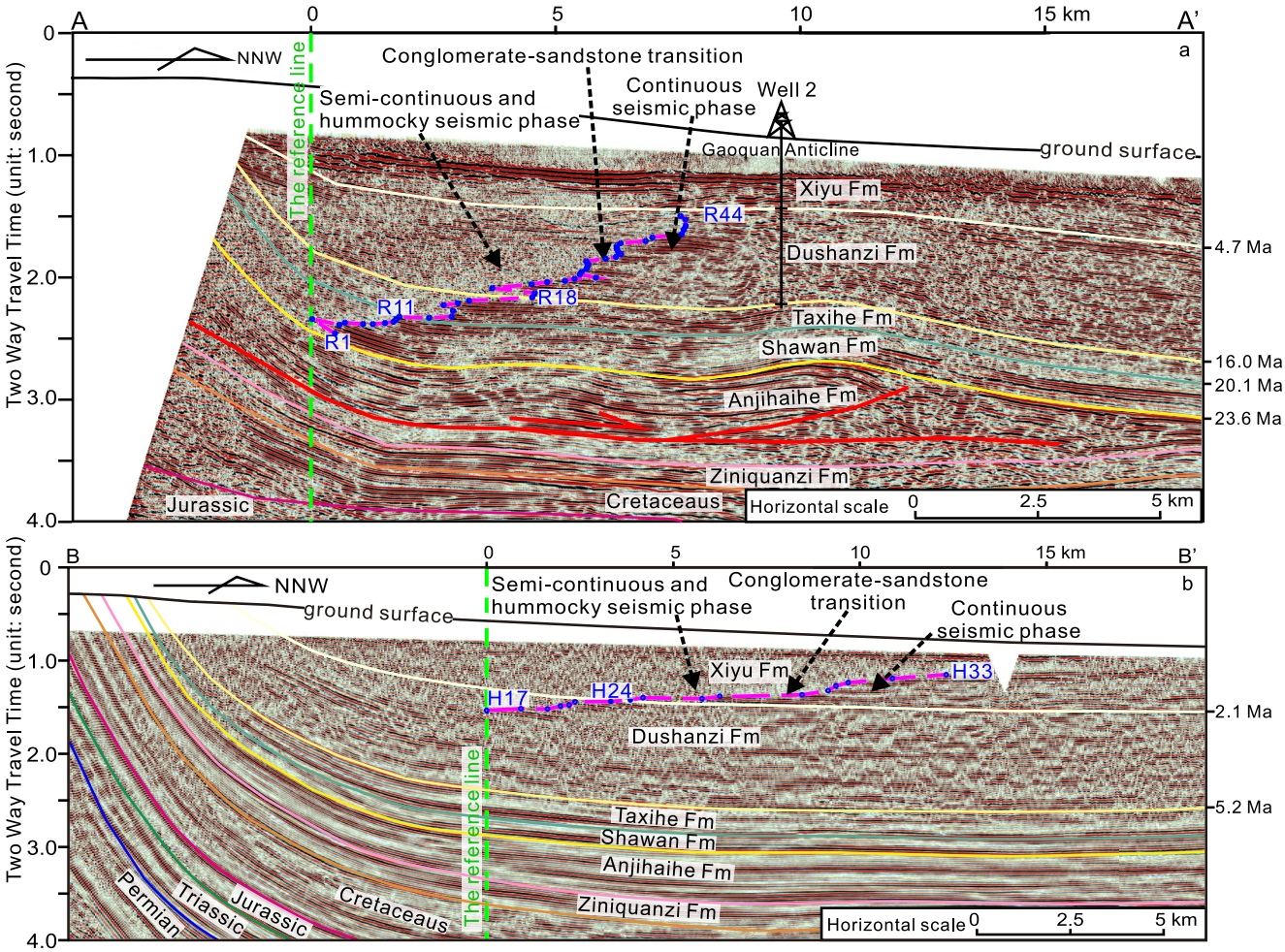

Figure 2. Interpreted near-north-south trending seismic profile AA′ (a) and BB′ (b) in the southern Junggar foreland basin. See Figure 1b for locations. See the original seismic profiles in Figures S1 and S5 in Supporting Information S1. The purple dashed lines indicate the traces of the conglomerate-sandstone transitions (CSTs) in deposit layers of the basin-fill. The green vertical lines marked the reference lines in the profiles. The horizontal resolution of these profiles is 0.1 km. The seismic phase transition between high amplitude, semicontinuous, hummocky phase and high amplitude, continuous phase occurs over a zone with a maximum width of 0.5 km. The formations' boundaries in the seismic profile are determined based on well logging data and outcropping geology near the profiles, and previous interpretations of seismic profiles in the basin (e.g., Qiu et al., 2019).

We locate the CST for each seismic reflector in the two profiles. We recognize 44 seismic reflectors in profile AA′, named R1 through R44 in ascending order (Figure 2a and Figure S1, Table S1 in Supporting Information S1). Reflectors R1–R10, R11–R17, and R18–R45 occur in the Shawan, Taxihe, and Dushanzi Fms, respectively (Figure 2a). The seismic phase contrast decreases to a level that cannot be identified from the upper Dushanzi Fm and the lower Xiyu Fm (Figure 2a). Four continuous parallel reflectors in the uppermost Xiyu Fm extend to the southern boundary of profile AA′, which may correspond to the Quaternary eolian beds in the northern front of the Tian Shan (Figure S4 in Supporting Information S1; Fang et al., 2002).

For profile BB′, we track 37 subparallel reflectors from the lower Dushanzi Fm to the middle Xiyu Fm, named H1 through H37 in ascending order to identify the CSTs (Figure 2b and Figure S5, Table S2 in Supporting Information S1). Yet, the top layer of the Xiyu Fm is not completely imaged in this profile.

We estimate the CST migration distance toward to the north (Figure 2). Since profiles AA′ and BB′ trend obliquely with respect to the strike of the northern Tian Shan range (Figure 1b), we project the distance of the CST migration in the direction perpendicular to the trend of the range (Figures 3a and 3b) to obtain the migration of the CSTs relative to the range. For profile AA′, the CST overall migrated 6.8 ± 0.5 km northward perpendicular to the range, from R2, the bottom of the Shawan Fm to R43, the top of the Dushanzi Fm. It is also noted that six

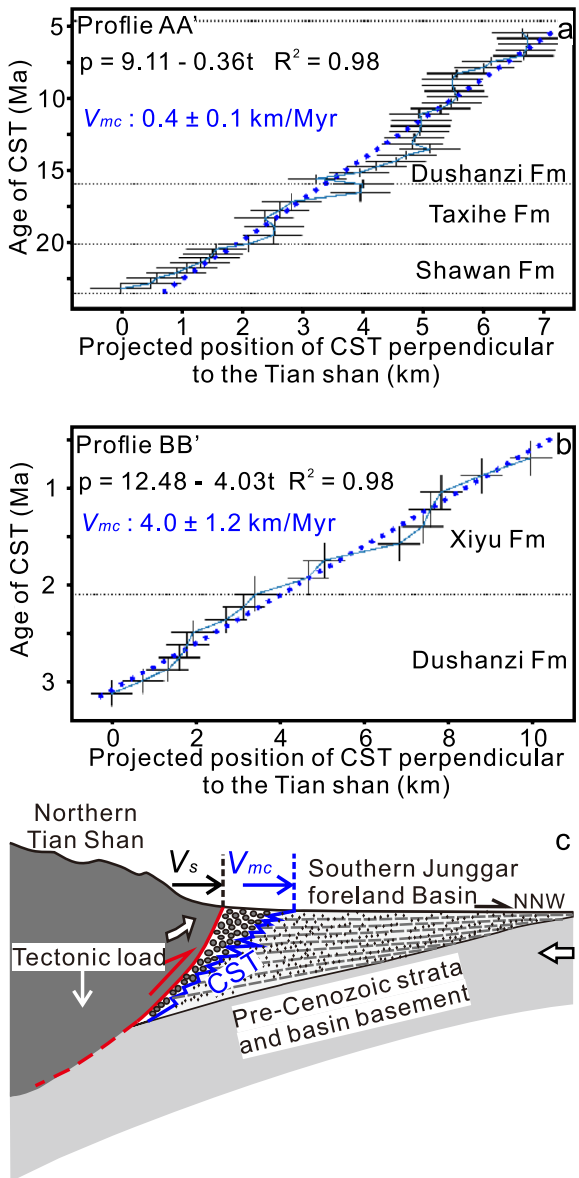

Figure 3. The linear-regression models of the projected positions (p) of the conglomerate-sandstone transitions (CSTs) along the direction perpendicular to the northern Tian Shan and their ages (t) from profile AA′ (a) and BB′ (b). Observed positions of the CSTs are indicated by the light blue solid lines, and the deep blue dashed lines mark the fitted lines. The black crosses indicate the uncertainties of p and t. (c) Schematic sketch of the relationship of the CST migration rates (V_{mc}) and the shortening rate of the thrust front relative to the foreland basin basement (V_s) in the northern Tian Shan orogen-foreland basin system. The sketch also shows that the tectonic load of the northern Tian Shan drives the flexural subsidence in the foreland basin.

episodes of southward retreat are superimposed on the overall northward migration (Figure 3a). For profile BB′, the CST migrated 10.0 ± 0.5 km northward perpendicular to the range, from H17 in the middle Dushanzi Fm to H33 in the lower Xiyu Fm.

Recent magnetostratigraphic studies of the Cenozoic strata in the southern Junggar foreland thrust-fold belt provide a chronostratigraphic framework (Figure 1b; Charreau et al., 2005; Charreau, Chen, et al., 2009; Lu et al., 2010). The Kuitun river (Charreau et al., 2005) and Taxi river (Lu et al., 2010) sections are closest to profiles AA′ and BB′, respectively (see location in Figure 1), and have several reliable anchoring points. We correlate the late Cenozoic strata imaged by profiles AA′ and BB′ (Figure 2) with those in the nearest magnetostratigraphically dated sections (Charreau et al., 2005; Charreau, Chen, et al., 2009; Lu et al., 2010) to assign an age for each recognized seismic reflector (see details in Supporting Information S1). The bottoms of the Shawan, Taxihe, Dushanzi, and Xiyu Fms in profile AA′ are dated at ~23.6, ~20.1, ~16, and ~4.7 Ma, respectively (Charreau et al., 2005; Charreau, Chen, et al., 2009; Figure 2a). The bottoms of the Dushanzi and Xiyu Fms in profile BB′ are dated at ~5.2 and ~2.1 Ma, respectively (Lu et al., 2010, Figure 2b). Assuming a constant sedimentation rate between two consecutive reflectors in one formation since the same formation shares a quasi-equal seismic wave velocity (Onajite, 2014), the age of all recognized seismic reflectors in the Shawan thorough Xiyu Fms were interpolated (Tables S1 and S2 in Supporting Information S1).

To examine spatial and temporal variations of the CSTs, we plot the projected positions (p) of the CSTs and their ages (t; Figures 3a and 3b). The linear-regression analysis of the CSTs from profile AA′ (Figure 3a) yields:

$$p = 9.112 - 0.36t, \quad R^2 = 0.98. \tag{1}$$

The linear-regression analysis of the CSTs from profile BB′ (Figure 3b) yields:

$$p = 12.475 - 4.03t, \quad R^2 = 0.98. \tag{2}$$

These results suggest that the CST migrated to the north in the direction perpendicular to the northern Tian Shan at a rate of 0.4 ± 0.1 mm/yr during the period from ~23 to ~6 Ma based on profile AA', and at a rate of 4.0 ± 1.2 mm/yr during the period from ~3.1 to ~0.7 Ma based on profile BB' (see details of migration rate uncertainty calculation in the Supporting Information S1). The deviation of a CST from the regression line is obtained by subtracting the linear-regression predicted positions from the corresponding observed positions. The positive deviation indicates more northward advance of a CST than their predicted positions; and the negative value means southward retreat of a CST with respect to the predicted ones (Figure 4).

4. Discussion

4.1. Implications for Cenozoic Growth of the Northern Tian Shan

Our results demonstrate that the two CSTs in this study migrated northward in the northern Tian Shan foreland basin system at steady rates since the early Miocene. The CSTs migrated at a rate of 0.4 ± 0.1 mm/yr along 84°E from ~23 to ~6 Ma and 4.0 ± 1.2 mm/yr along 87°E from ~3.1 to ~0.7 Ma (V_{mc} in Figure 3c). These steady rates suggest a long-term (10^6 year-timescale) stability of the geological process responsible for their migration. The dominant process controlling the migration of the CSTs is the forelandward propagation of the northern Tian Shan orogenic wedge (e.g., Avouac et al., 1993;

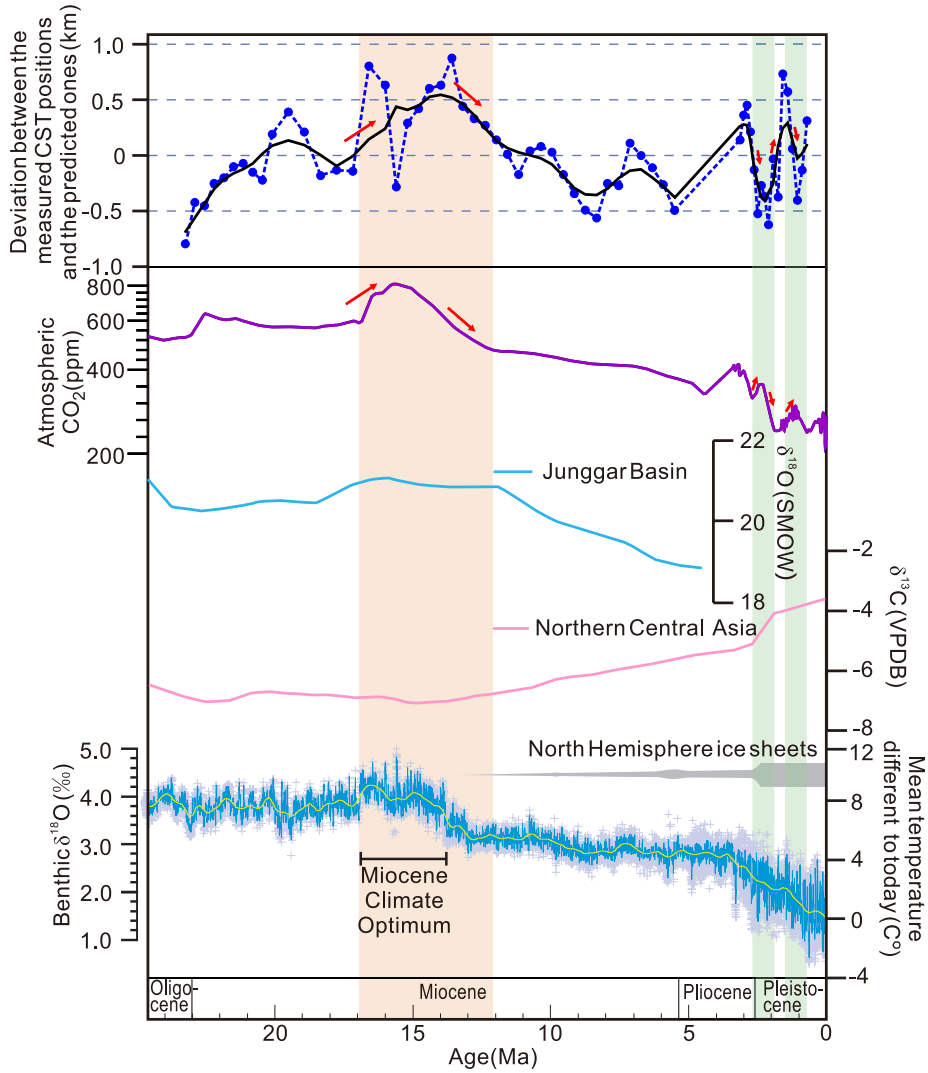

Figure 4. Deviations between the measured conglomerate-sandstone transition (CST) positions and the predicted ones in the southern Junggar foreland basin infill (dark blue dotted line) with lowness smooth shown in the black solid curve, atmospheric CO_2 reconstructions from boron isotopes (purple solid curve) (Rae et al., 2021), pedogenic carbonates $\delta^{18}O$ from the Junggar Basin (light blue solid line) (Caves Rugenstein & Chamberlain, 2018; Charreau et al., 2012), pedogenic carbonate $\delta^{13}C$ from the northern Central Asia (pink solid curve) (Caves Rugenstein & Chamberlain, 2018), and surface temperature variations estimated from the global deep-sea oxygen isotope record (yellow solid line) since ~24 Ma (Westerhold et al., 2020). Temperatures in the northern Central Asia are derived from data collected in Mongolia, Junggar Basin, Kazakhstan, and Kyrgyzstan (Caves Rugenstein & Chamberlain, 2018). The light green bands highlight the periods with inverse correlations between the deviations and atmospheric CO_2 variations. SMOW—standard mean ocean water; VPDB—Vienna Peedee belemnite.

Wang et al., 2013). The analyses of the structural geometry and kinematics of the southern Junggar foreland fold-thrust belt (SJFFTB) also reveal the gradual northward thrusting of the orogenic wedge since early Miocene (e.g., Avouac et al., 1993; Qiu et al., 2019). Based on the deformation of the Neogene strata in the south of the basin and its thinning at the mountain front (Figure 1c and Figures S1, S5 in Supporting Information S1), this thrusting has been ongoing throughout accumulation of the CSTs. Hence, these constant rates suggest a long-term (10^6 year-timescale) flux steady state system (Willett & Brandon, 2002) in response to continuous crustal shortening across the northern Tian Shan (Figure 3c). Therefore, we consider the migration rates of the CSTs (V_{mc} in Figure 3c) as a proxy for shortening of the northern Tian Shan thrust front relative to the Junggar Basin basement (V_s in Figure 3c) assuming a steady state orogenic wedge-foreland basin system (Armitage et al., 2011; Burbank et al., 1988; Dubille & Lavé, 2015; Sinclair & Naylor, 2012).

Nevertheless, there is an order of magnitude difference in the migration rates between profile AA′ and BB′, which disagrees with the observed eastward decrease in shortening in the northern Tian Shan (Avouac et al., 1993; Wang & Shen, 2020). This discrepancy is possibly related to the tectonics in the northern margin of the Tian Shan, considering that there is no significant change in sedimentation rates in the basin from ~6 to ~3 Ma (Charreau et al., 2005; Charreau, Chen, et al., 2009). The northern Tian Shan is bounded by the Dzungarian right-lateral strike-slip fault (BGMRX, 1993; Campbell et al., 2013; Hu et al., 2021) to the west of ~83°30′E and by the SJFFTB to the east of ~83°30′E (Figure 1b; BGMRX, 1993). Profile AA′ is located near the junction between the Dzungarian fault and the SJFFTB, implying that the contractional structures in the western northern Tian Shan solely absorbed a portion of the shortening that was partitioned during transpressional tectonism (Figure 1b). In contrast, profile BB′ lies near the middle segment of the SJFFTB; the contractional structures in this segment represent the total shortening of the thrust wedge (Qiu et al., 2019). Therefore, it is feasible that the CST migration rate derived from profile BB′ is an order of magnitude higher than that from profile AA′; and we conclude that the rate from profile BB′ represents the first-order, long-term shortening between the northern Tian Shan thrust front and the Junggar Block. The rate from profile BB′ is comparable to the average Quaternary shortening rate of the middle segment of the thrust-fold belt, 3.9 ± 0.4 mm/yr, based on balanced section studies (Qiu et al., 2019; see location in Figure 1b) and the shortening rate of the modern northern Tian Shan along 87°E, 4.0 ± 1.4 mm/yr, from geodetic measurements (Yang et al., 2008).

4.2. Climatic Impacts on CST Migration

The variations of the measured CST positions relative to the linear regression suggest other processes superimposed on the tectonically driven, long-term northward migration of the CSTs. The deviation is qualitatively similar to the patterns of global atmospheric CO_2 and surface temperature variations over the past 23 million years (Rae et al., 2021; Westerhold et al., 2020; Figure 4).

The deviation positively correlates with global atmospheric CO_2 and temperature variations before ~6 Ma but negatively with atmospheric CO_2 changes after ~3 Ma (Figure 4). The different correlations could be related to the different agents of sediment transport and physical erosion in the northern Tian Shan before and after the late Miocene. Before ~6 Ma, northern Hemisphere ice sheets have not fully established (Westerhold et al., 2020; Zachos et al., 2001). In this stage, the stable alpine glaciers in the northern Tian Shan range had not formed, so the fluvial system could be the dominant agent of sediment transport (Charreau et al., 2011). The positive peak of the deviation during ~14–17 Ma coincides with the Middle Miocene Climatic Optimum (Figure 4; Zachos et al., 2001), enhancement of precipitation in the northern Tian Shan during ~14–17 Ma as revealed by the forest environment (Ye et al., 2012), and the increase in both oxygen and carbon isotopic values of the lacustrine sediments during this period (Charreau et al., 2012). The enhanced moisture supply carried by Westerlies and Asian Monsoon can induce hydrological changes and enhanced incision (e.g., Malatesta et al., 2018) to advance the CSTs further northward than the predicted ones when atmospheric CO_2 and temperature rose before ~6 Ma. The strong alpine glacier erosion appeared in the northern Tian Shan in the Quaternary, as revealed by a transient increase in the physical erosion rates at the onset of Quaternary glaciations (Charreau et al., 2011). The CST position hence was significantly affected by glacier erosion after ~3 Ma since the glacier erosion became the dominant erosion agent (Malatesta et al., 2018). The widespread glaciation can drive higher rates of erosion and sediment production than fluvial erosion to advance the CST further northward than the predicted ones (Shi et al., 2006; Shuster et al., 2005; Figure S7 in Supporting Information S1) when the glaciers expanded as atmospheric CO_2 and temperature dropped after ~3 Ma.

The deviation is also consistent with the lacustrine carbonate stable oxygen isotope data ($\delta^{18}O$) from the Junggar Basin (Figure 4; Caves et al., 2017; Charreau et al., 2012) and is in opposite phase with the pedogenic stable carbon isotope one ($\delta^{13}C$) from the northern Central Asia (Caves Rugenstein & Chamberlain, 2018).The consistency of the deviation with the stable oxygen and carbon isotope data in this region supports the secondary role of atmospheric CO_2 and temperature variation on the control of CST migration considering that atmospheric circulation in the northern Central Asia is tightly controlled by global climate in the late Cenozoic (Caves et al., 2017).

This phenomenon suggests that the second-order CST migration in the basin was probably regulated by climate changes. Other influencing factors on the migration of the CST are deemed minor and cannot be qualitatively distinguished.

5. Conclusions

The two seismic profiles in the southern Junggar foreland basin show that the CSTs in the basin-fill migrated northward at a rate of 0.4 ± 0.1 mm/yr along the longitude of 84°E from ~23 to ~6 Ma and at 4.0 ± 1.2 mm/yr along 87°E from ~3.1 to ~0.7 Ma. The rates approximate the long-term shortening rates in the northern Tian Shan orogen-foreland basin system. An order of magnitude difference between these two rates along the eastern and western profiles indicates the lateral variations of the strain allocation between the north-south shortening and the northwest dextral strike-slip faulting along the range. Temporal deviations in the CST positions are qualitatively comparable to variations in atmospheric CO_2 and surface temperatures over the past ~23 million years, implying that the second-order CST migrations are likely regulated by climatic changes.

Data Availability Statement

The original seismic data supporting this research are owned by the China National Petroleum Corporation (CNPC) with commercial restrictions and is not accessible to the public or research community. The high-resolution seismic profiles used in this study can be accessed via: https://doi.org/10.6084/m9.figshare.18218120.v2. The python code for linear-regression analysis and lowness smooth is archived at https://doi.org/10.6084/m9.figshare.18218120.v2.

Acknowledgments
This work was supported by National Key R&D Plan (Grant No. 2017YFC0601402), the National Natural Science Foundation of China (Grant Nos. 41672198, 42072153, and 42102250), and the Fundamental Research Funds for the Central Universities (Grant No. B200201025). Zhipeng Diao participated the field trip. This study benefited from discussion with Dr. Yanjun Wang and Profs. Shaowen Liu and Jinbao Su. We also thank Editor Lucy Flesh and Dr. Gilby Jepson for their detailed and insightful reviews.

References

Allen, P. A., Armitage, J. J., Carter, A., Duller, R. A., Michael, N. A., Sinclair, H. D., et al. (2013). The Qs problem: Sediment volumetric balance of proximal foreland basin systems. *Sedimentology*, *1*, 102–130. https://doi.org/10.1111/sed.12015

Armitage, J. J., Duller, R. A., Whittaker, A. C., & Allen, P. A. (2011). Transformation of tectonic and climatic signals from source to sedimentary archive. *Nature Geoscience*, *4*, 231–235. https://doi.org/10.1038/ngeo1087

Avouac, J. P., Tapponnier, P., Bai, M., You, H., & Wang, G. (1993). Active thrusting and folding along the northern Tien Shan and late Cenozoic rotation of the Tarim relative to Dzungaria and Kazakhstan. *Journal of Geophysical Research*, *98*, 6755–6804. https://doi.org/10.1029/92JB01963

BGMRX (Bureau of Geological and Mineral Resources of BGMRX the Xinjiang Uygur Autonomous Region). (1993). Regional geology of Xinjiang Uygur Autonomous region. in Chinese, (pp 1–841). Geology Publishing House.

Bullen, M. E., Burbank, D. W., Garver, J. I., & Abdrakhmatov, K. Y. (2001). Late Cenozoic tectonic evolution of the northwestern Tien Shan: New age estimates for the initiation of mountain building. *The Geological Society of America Bulletin*, *113*, 1544–1559. https://doi.org/10.1130/0016-7606(2001)113<1544:LCTEOT>2.0.CO;2

Burbank, D. W., Beck, R. A., Raynolds, H., Hobbs, R., & Tahirkheli, K. (1988). Thrusting and gravel progradation in foreland basins—A test of post-thrusting gravel dispersal. *Geology*, *16*, 1143–1146. https://doi.org/10.1130/0091-7613(1988)016<1143:TAGPIF>2.3.CO;2

Campbell, G. E., Walker, R. T., Abdrakhmatov, K., Schwenninger, J. L., Jackson, J., Elliott, J. R., et al. (2013). The Dzhungarian fault: Late Quaternary tectonics and slip rate of a major right-lateral strike-slip fault in the northern Tien Shan region. *Journal of Geophysical Research: Solid Earth*, *118*, 5681–5698. https://doi.org/10.1002/jgrb.50367

Caves, J. K., Bayshashov, B. U., Zhamangara, A., Ritch, A. J., Ibarra, D. E., Sjostrom, D. J., et al. (2017). Late Miocene uplift of the tian Shan and Altai and reorganization of central Asia climate. *Geological Society of America Today*, *27*, 19–26. https://doi.org/10.1130/GSATG305A.1

Caves Rugenstein, J. K., & Chamberlain, C. P. (2018). The evolution of hydroclimate in Asia over the Cenozoic: A stable-isotope perspective. *Earth-Science Reviews*, *185*, 1129–1156. https://doi.org/10.1016/j.earscirev.2018.09.003

Cawood, P. A., Kröner, A., Collins, W. J., Kusky, T. M., Mooney, W. D., & Windley, B. F. (2009). Accretionary orogens through earth history. *Geological Society, London, Special Publications*, *318*(1), 1–36. https://doi.org/10.1144/SP318.1

Charreau, J., Blard, P.-H., Puchol, N., Avouac, J.-P., Lallier-Vergès, E., Bourlès, D., et al. (2011). Paleo-erosion rates in central Asia since 9Ma: A transient increase at the onset of quaternary glaciations? *Earth and Planetary Science Letters*, *304*, 85–92. https://doi.org/10.1016/j.epsl.2011.01.018

Charreau, J., Chen, Y., Gilder, S., Dominguez, S., Avouac, J. P., Sen, S., et al. (2005). Magnetostratigraphy and rock magnetism of the Neogene Kuitun He section (northwest China): Implications for late Cenozoic uplift of the Tianshan mountains. *Earth and Planetary Science Letters*, *230*, 177–192. https://doi.org/10.1016/j.epsl.2004.11.002

Charreau, J., Chen, Y., Gumiaux, C., Gilder, S., Barrier, L., Dominguez, S., et al. (2009). Neogene uplift of the Tian Shan Mountains observed in the magnetic record of the Jingou River section (northwest China). *Tectonics*, *28*, TC2008. https://doi.org/10.1029/2007TC002137

Charreau, J., Gumiaux, C., Avouac, J. P., Augier, R., Chen, Y., Barrier, L., et al. (2009). The Neogene Xiyu Formation, a diachronous prograding gravel wedge at front of the Tianshan: Climatic and tectonic implications. *Earth and Planetary Science Letters*, *287*, 298–310. https://doi.org/10.1016/j.epsl.2012.05.033

Charreau, J., Kent-Corson, M. L., Barrier, L., Augier, R., Ritts, D. B., Chen, Y., et al. (2012). A high-resolution stable isotopic record from the Junggar Basin (NWChina): Implications for the paleotopographic evolution of the Tianshan Mountains. *Earth and Planetary Science Letters*, *341*, 158–169. https://doi.org/10.1016/j.epsl.2012.05.033

Charvet, J., Shu, L. S., Laurent-Charvet, S., Wang, B., Faure, M., Cluzel, D., et al. (2011). Paleozoic tectonic evolution of the Tianshan belt, NW China. *Science China: Earth Science*, *54*, 166–184. https://doi.org/10.1007/s11430-010-4138-1

DeCelles, P. G., & DeCelles, P. C. (2001). Rates of shortening, propagation, underthrusting, and flexural wave migration in continental orogenic systems. *Geology*, *29*, 135–138. https://doi.org/10.1130/0091-7613(2001)029<0135:ROSPUA>2.0.CO;2;2

Dingle, E. H., Attal, M., & Sinclair, H. D. (2017). Abrasion-set limits on Himalayan gravel flux. *Nature*, *544*, 471–474. https://doi.org/10.1038/nature22039

Dingle, E. H., Sinclair, H. D., Attal, M., Milodowski, D. T., & Singh, V. (2016). Subsidence control on river morphology and grain size in the Ganga Plain. *American Journal of Science*, *316*, 778–812. https://doi.org/10.2475/08.2016.03

Dubille, M., & Lavé, J. (2015). Rapid grain size coarsening at sandstone/conglomerate transition: Similar expression in Himalayan modern rivers and Pliocene molasse deposits. *Basin Research*, *27*, 26–42. https://doi.org/10.1111/bre.12071

Duller, R. A., Whittaker, A. C., Fedele, J. J., Whitchurch, A. L., Springett, J., Smithells, R., et al. (2010). From grain size to tectonics. *Journal Geophysical Research*, *115*, F03022. https://doi.org/10.1029/2009JF001495

Dumitru, T. A., Zhou, D., Chang, E. Z., Graham, S. A., Hendrix, M. S., Sobel, E. R., et al. (2001). Uplift, exhumation, and deformation in the Chinese Tian Shan). *Uplift, exhumation, and deformation in the Chinese Tian Shan* (pp. 71–100). Memoirs-Geological Society of America. https://doi.org/10.1130/0-8137-1194-0.71

Fang, X., Shi, Z., Yang, S., Yan, M. D., Li, J., & Jiang, P. (2002). Loess in the Tian Shan and its implications for the development of the Gurbantunggut desert and drying of northern Xinjiang. *Chinese Science Bulletin*, *16*, 1381–1387. https://doi.org/10.1360/02tb9305

Ferguson, R., Hoey, T., Wathen, S., & Werritty, A. (1996). Field evidence for rapid downstream fining of river gravels through selective transport. *Geology*, *24*, 179–182. https://doi.org/10.1130/0091-7613(1996)024<0179:FEFRDF>2.3.CO;2

Flemings, P. B., & Jordan, T. E. (1989). A synthetic stratigraphic model of Foreland Basin development. *Journal of Geophysical Research*, *94*, 3851–3866. https://doi.org/10.1029/JB094iB04p03851

He, D., Suppe, J., Geng, Y., Shuwei, G., Shaoying, H., Xin, S., et al. (2005). Guide book for field trip in south and north Tianshan foreland basin, Xinjiang Uygur Autonomous Region, China. In *International conference on theory and application of fault-related folding in foreland basins* (pp. 77).

Hendrix, M. S., Graham, S. A., Carroll, A. R., Sobel, E. R., McKnight, C. L., Schulein, B. J., et al. (1992). Sedimentary record and climatic implications of recurrent deformation in the Tian Shan: Evidence from Mesozoic strata of the north Tarim, south Junggar, and Turpan basins, northwest China. *GSA Bulletin*, *104*(1), 532–579. https://doi.org/10.1130/0016-7606(1992)104<0053:SRACIO>2.3.CO;2

Hu, Z., Yang, X., Yang, H., Huang, W., Wu, G., Miao, S., et al. (2021). Slip rate and paleo seismology of the Bolokenu-Aqikekuduk (Dzhungarian) right-lateral strike-slip fault in the northern Tian Shan, NW China. *Tectonics*, *40*, e2020TC006604. https://doi.org/10.1029/2020TC006604

Jepson, G., Glorie, S., Khudoley, A., Malyshev, S., Gillespie, J., Glasmacher, U., et al. (2021). The Mesozoic exhumation history of the Karatau-Talas range, western Tian Shan, Kazakhstan-Kyrgyzstan. *Tectonophysics*, *814*, 228977. https://doi.org/10.1016/j.tecto.2021.228977

Jepson, G., Glorie, S., Konopelko, D., Gillespie, J., Danišík, M., Mirkamalov, R., et al. (2018). Low-temperature thermochronology of the Chatkal-Kurama terrane (Uzbekistan-Tajikistan): Insights into the Meso-Cenozoic thermal history of the western Tian Shan. *Tectonics*, *37*, 3954–3969. https://doi.org/10.1029/2017TC004878

Jolivet, M., Dominguez, S., Charreau, J., Chen, Y., Li, Y., & Wang, Q. (2010). Mesozoic and Cenozoic tectonic history of the central Chinese tian Shan: Reactivated tectonic structures and active deformation. *Tectonics*, *29*, TC6019. https://doi.org/10.1029/2010TC002712

Li, C., Wang, S. L., Naylor, M., Sinclair, H., & Wang, L. S. (2020). Evolution of the Cenozoic Tarim Basin by flexural subsidence and sediment ponding: Insights from quantitative basin modelling. *Marine and Petroleum Geology*, *112*, 104047. https://doi.org/10.1016/j.marpetgeo.2019.104047

Li, C., Wang, S. L., & Wang, L. S. (2019). Tectonostratigraphic history of the southern Tianshan, China: Seismic profiling evidence. *Journal of Asian Earth Sciences*, *1*, 101–114. https://doi.org/10.1016/j.jseaes.2018.08.017

Lu, H. H., Burbank, W. D., Li, Y. L., & Liu, Y. M. (2010). Late Cenozoic structural and stratigraphic evolution of the northern Chinese Tian Shan foreland. *Basin Research*, *22*, 249–269. https://doi.org/10.1111/j.1365-2117.2009.00412.x

Lv, R. (2005). *The relationship between tectonic evolution of intracontinental foreland basin and Oil-gas in southern margin of Junggar Basin* (Master's dissertation, in Chinese with English Abstract). China National Knowledge Infrastructure. China University of Geosciences.

Macaulay, E. A., Sobel, E. R., Mikolaichuk, A., Landgraf, A., Kohn, B., & Stuart, F. (2013). Thermochronologic insight into late Cenozoic deformation in the basement-cored Terskey Range, Kyrgyz Tien Shan. *Tectonics*, *32*, 487–500. https://doi.org/10.1002/tect.20040

Malatesta, C. L., Avouac, J.-P., Brown, D. N., Breitenbach, F. S., Pan, J. W., Chevalier, M.-L., et al. (2018). Lag and mixing during sediment transfer across the Tian Shan piedmont caused by climate-driven aggradation–incision cycles. *Basin Research*, *30*, 613–635. https://doi.org/10.1111/bre.12267

Molnar, P., & Tapponnier, P. (1975). Cenozoic tectonics of Asia: Effects of a continental collision. *Science*, *189*(4201), 419–426. https://doi.org/10.1126/science.189.4201.419

Onajite, E. (2014). *Seismic data analysis techniques in hydrocarbon exploration* (pp. 178–210). Elsevier's Science & Technology Rights Department. https://doi.org/10.1016/C2013-0-09969-0

Paola, C., Heller, P. L., & Angevine, C. L. (1992). The large-scale dynamics of grain-size variation in alluvial basins, 1: Theory. *Basin Research*, *4*, 73–90. https://doi.org/10.1111/j.1365-2117.1992.tb00145.x

Qiu, J. H., Rao, G., Wang, X., Yang, D. S., & Xiao, L. X. (2019). Effects of fault slip distribution on the geometry and kinematics of the southern Junggar fold-and-thrust belt, northern Tian Shan. *Tectonophysics*, *772*, 228209. https://doi.org/10.1016/j.tecto.2019.228209

Quick, L., Sinclair, H. D., Attal, M., & Singh, V. (2020). Conglomerate recycling in the Himalayan foreland basin: Implications for grain size and provenance. *The Geological Society of America Bulletin*, *132*, 1639–1656. https://doi.org/10.1130/b35334.1

Rae, W. J., Zhang, Y. G., Liu, X. Q., Foster, L. G., Stoll, M. H., & Whiteford, D. R. (2021). Atmospheric CO_2 over the Past 66 Million Years from marine archives. *Annual Review of Earth and Planetary Sciences*, *49*, 609–641. https://doi.org/10.1146/annurev-earth-082420-063026

Schlunegger, F., & Norton, K. (2015). Climate vs. tectonics: The competing roles of Late Oligocene warming and Alpine orogenesis in constructing alluvial megafan sequences in the North Alpine foreland basin. *Basin Research*, *27*, 230–245. https://doi.org/10.1111/bre.12070

Shi, Y. F., Cui, Z. J., & Su, Z. (2006). *The quaternary glaciations and environmental variations in China* (pp. 1–618). Hebei, Science and Technology Press.

Shuster, D. L., Ehlers, T. A., Rusmore, M. E., & Farley, K. A. (2005). Rapid glacial erosion at 1.8 Ma revealed by 4He/3He thermochronometry. *Science*, *310*, 1668–1670. https://doi.org/10.1126/science.1118519

Sinclair, H. D., Coakley, B. J., Allen, P. A., & Watts, A. B. (1991). Simulation of foreland basin stratigraphy using a diffusion model of mountain belt uplift and erosion: An example from the central Alps, Switzerland. *Tectonics*, *10*, 599–620. https://doi.org/10.1029/90TC02507

Sinclair, H. D., & Naylor, M. (2012). Foreland basin subsidence driven by topographic growth versus plate subduction. *The Geological Society of America Bulletin*, *124*, 368–379. https://doi.org/10.1130/B30383.1

Sobel, E. R., Chen, J., & Heermance, R. V. (2006). Late Oligocene-Early Miocene initiation of shortening in the Southwestern Chinese Tian Shan: Implications for Neogene shortening rate variations. *Earth and Planetary Science Letters*, *247*(1–2), 70–81. https://doi.org/10.1016/j.epsl.2006.03.048

Wang, S. L., Chen, Y., Charreau, J., Wei, D. T., & Jia, D. (2013). Tectono-stratigraphic history of the southern Junggar Basin: Seismic profiling evidences. *Terra Nova*, *25*, 490–495. https://doi.org/10.1111/ter.12063

Wang, M., & Shen, Z. K. (2020). Present-day crustal deformation of continental China derived from GPS and its tectonic implications. *Journal of Geophysical Research: Solid Earth*, *125*, e2019JB018774. https://doi.org/10.1029/2019JB018774

Westerhold, T., Marwan, N., Drury, J. A., Liebrand, D., Agnini, C., Anagnostou, E., et al. (2020). An astronomically dated record of Earth's climate and its predictability over the last 66 million years. *Science*, *369*, 1383–1387. https://doi.org/10.1126/science.aba6853

Willett, S. D., & Brandon, M. T. (2002). On steady states in mountain belts. *Geology*, *30*, 175–178. https://doi.org/10.1130/0091-7613(2002)030<0175:OSSIMB>2.0.CO;2

Windley, B. F., Allen, M. B., Zhang, C., Zhao, Z. Y., & Wang, G. R. (1990). Paleozoic accretion and Cenozoic deformation of the Chinese Tien Shan Range, central Asia. *Geology*, *18*, 128–131. https://doi.org/10.1130/0091-7613(1990)018<0128:PAACRO>2.3.CO;2

Yang, S., Li, J., & Wang, Q. (2008). The deformation pattern and fault rate in the Tianshan Mountains inferred from GPS observations. *Science China Earth Sciences*, *51*, 1064–1080. https://doi.org/10.1007/s11430-008-0090-8

Ye, J., Wu, W. Y., Ni, X. J., Bi, S. D., Sun, J. M., & Meng, J. (2012). The Duolebulejin section of northern Junggar Basin and its stratigraphic and environmental implication (in Chinese). *Science China Earth Sciences*, *10*, 1523–1532. https://doi.org/10.1007/s11783-011-0280-z

Zachos, J., Pagani, M., Sloan, L., Thomas, E., & Billups, K. (2001). Trends, rhythms, and aberrations in global climate 65 Ma to present. *Science*, *292*, 686–693. https://doi.org/10.1126/science.1059412